THE JOURNAL OF PHYSICAL CHEMISTRY C

Article

pubs.acs.org/JPCC

Sensitivity of the Mott–Schottky Analysis in Organic Solar Cells

Thomas Kirchartz,*[†] Wei Gong,[†,§] Steven A. Hawks,[‡] Tiziano Agostinelli,[†] Roderick C. I. MacKenzie,[†] Yang Yang,[‡] and Jenny Nelson[†]

[†]Department of Physics, Imperial College London, South Kensington SW7 2AZ, United Kingdom

[‡]Department of Materials Science and Engineering, University of California, Los Angeles, Los Angeles, California 90095, United States

[§]Key Laboratory of Luminescence and Optical Information, Ministry of Education and Institute of Optoelectronics Technology, Beijing Jiaotong University, Beijing 100044, People's Republic of China

Supporting Information

ABSTRACT: The application of Mott–Schottky analysis to capacitance–voltage measurements of polymer:fullerene solar cells is a frequently used method to determine doping densities and built-in voltages, which have important implications for understanding the device physics of these cells. Here we compare drift-diffusion simulations with experiments to explore the influence and the detection limit of doping in situations where device thickness and doping density are too low for the depletion approximation to be valid. The results of our simulations suggest that the typically measured values on the order of 5×10^{16} cm^{-3} for doping density in thin films of 100 nm or lower may not be reliably determined from capacitance measurements and could originate from a completely intrinsic active layer. In addition, we explain how the violation of the depletion approximation leads to a strong underestimation of the actual built-in voltage by the built-in voltage V_{MS} determined by Mott–Schottky analysis.

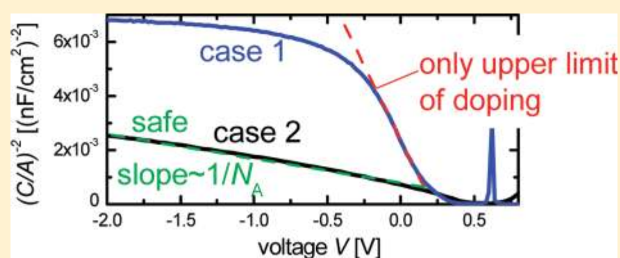

I. INTRODUCTION

A thorough understanding of the device physics of polymer-based solar cells[1−7] is a crucial prerequisite for purposeful optimization of these devices and materials. Stimulated by the study of capacitance/voltage (CV) measurements done on polythiophene:fullerene solar cells, there has been a recent debate about the correct band diagram of polymer:fullerene bulk heterojunction cells and in particular about the relevance and magnitude of doping and contact barriers.[8,9] CV measurements are a well established tool to determine the doping density and the built-in voltage of Schottky or $p-n$ junctions. Application of the standard Mott–Schottky analysis[10,11] to polythiophene:fullerene solar cells led to doping densities $N_A \approx 10^{16}$ cm^{-3} attributed to oxygen and moisture[12,13] and built-in voltages V_{bi} that were often on the order of 400 mV or below.[13−17] From these measurements, refs 9, 13−15, and 18 inferred that the band diagram for the studied cells was that of a doped layer and a Schottky junction at the back contact adjacent to the Al back contact as shown in Figure 1a. This band diagram deviates from that used by most groups working on the drift-diffusion modeling of bulk-heterojunction devices,[19−29] which usually assume an intrinsic absorber layer with one Schottky junction toward the metal and another one toward the poly(3,4-ethylenedioxythiophene):poly(styrenesulfonate) (PEDOT:PSS) hole transporting layer as shown in Figure 1b. These Schottky junctions are usually assumed to have a low or even zero Schottky barrier;[30] that is, the anode is assumed to be a good hole injector and the cathode is assumed to be a good electron injector. Although the CV measurements seem to prove the band diagram in Figure 1b wrong, the low values for the built-in voltage as determined from Mott–Schottky analysis of CV measurements raise the question of how $V_{bi} < 400$ mV can be consistent with $V_{oc} > 500$ mV, which could only be possible in the presence of selective contacts. However, in a device with selective contacts, where $V_{oc} > V_{bi}$ is possible, the fill factor would suffer drastically from the low V_{bi} since the photogenerated charge carriers have to diffuse against the electric field to be collected at the contact. Thus, it can be assumed that no efficient organic solar cell can exist with a reasonable fill factor which has a built-in voltage that is considerably smaller than its open circuit voltage. In addition, it has remained unclear how an intrinsic or low doped thin semiconductor film with two space charge regions on either side would behave in a CV measurement and, thus, under which circumstances Mott–Schottky analysis is actually sensitive to the differences between the band diagrams in Figure 1a,b.

In this article, we study the voltage dependence of the capacitance of the two band diagrams in Figure 1 by means of frequency domain drift diffusion simulations using the software SCAPS[31−35] and compare the simulations with experimental results on poly (3-hexylthiophene) (P3HT): 1-(3-

Received: January 12, 2012
Revised: February 28, 2012

 © XXXX American Chemical Society dx.doi.org/10.1021/jp300397f | J. Phys. Chem. C XXXX, XXX, XXX−XXX

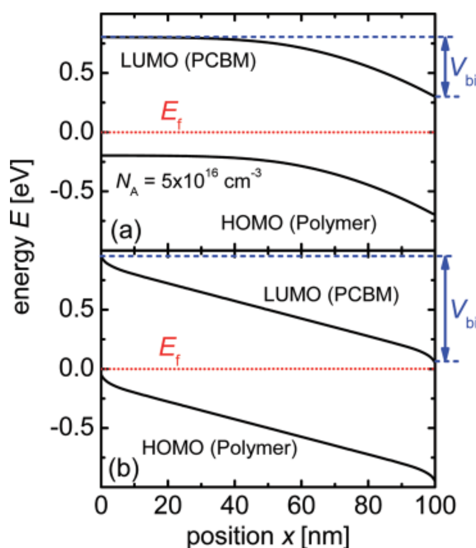

Figure 1. Comparison of the two band diagrams that are currently considered for polymer:fullerene solar cells. In both cases, the traditional role of the valence band in a crystalline semiconductor is associated with the polymer highest occupied molecular orbital (HOMO), while the conduction band is associated with the fullerene lowest unoccupied molecular orbital (LUMO). (a) Band diagram of a doped semiconductor with a flatband front contact and a Schottky junction with space charge region at the back contact. (b) Band diagram of an intrinsic solar cell with two Schottky junctions and two space charge regions on both sides.

methoxycarbonyl)propyl-1-phenyl-[6,6]-methano fullerene (PCBM) solar cells in a normal device geometry with the layer sequence glass/ITO/PEDOT:PSS/P3HT:PCBM/(Ca)/Al.[36,37] We determine the apparent doping density of intrinsic absorber layers as a function of thickness and show that especially for thin intrinsic films around 100 nm or below, substantial apparent doping densities on the order of $N_A \approx 10^{16}$ cm^{-3} result from Mott−Schottky analysis. This shows that depending on thickness and actual doping density, the use of Mott−Schottky analysis can lead to erroneous results. However, we also explain under which circumstances the determination of the doping density is safe. In addition, we show that Mott−Schottky analysis is not sensitive to any band bending due to free charge injected from the contact. Thus, a possible second space charge region at the PEDOT:PSS interface and any band bending due to injected electrons at the metal contact are not detected. In consequence, the actual built-in voltage can be much larger than the one determined from Mott−Schottky analysis.

II. BASIC THEORY OF THE MOTT−SCHOTTKY ANALYSIS

The standard analysis of capacitance−voltage scans in Schottky junctions with doped semiconductors is based on the depletion approximation, which implies that there are no free carriers in the space charge region at the junction under investigation. Thus, the charge in the space charge region is entirely due to dopant atoms or molecules. By modulating the width w of the space charge region by changing the applied DC bias, the capacitance

$$C = \frac{\varepsilon_0 \varepsilon_r A}{w} \tag{1}$$

of the space charge region is modulated as well. Here, ε_0 is the dielectric constant of vacuum, ε_r is the relative dielectric constant of the doped semiconductor, and A is the area. The space charge width depends on the doping density and the built-in voltage V_{bi} via

$$w = \sqrt{\frac{2\varepsilon(V_{bi} - V)}{qN_A}} \tag{2}$$

where $\varepsilon = \varepsilon_r\varepsilon_0$ and N_A is the doping density. Thus, the so-called Mott−Schottky plot of C^{-2} versus applied DC voltage yields a straight line, whose slope yields the doping density and whose extrapolated intersection with the voltage axis yields the built-in voltage. The doping density

$$N_A(x) = -\frac{2}{q\varepsilon A}\left(\frac{dC(x)^{-2}}{dV}\right)^{-1} \tag{3}$$

can also be determined as a function of distance x from the junction if the result of eq 3 is plotted vs $x = \varepsilon A/C$. Note that in all following examples, we consider "normal" geometries for organic solar cells, where the hole injecting and extracting contact is at $x = 0$, and p-type doping, meaning that the main junction is at the back contact as shown in Figure 1a. In this case $x = d - \varepsilon A/C$, where x is now measured from the front contact and d is the device thickness.

To avoid confusion between parameters that are input for simulations and parameters that are the output of the Mott−Schottky analysis of either simulated or measured data, we will use different symbols in the remainder of the article. While the input parameters for the simulation will be N_A for the acceptor concentration and V_{bi} for the built-in voltage, the apparent doping density as determined by the Mott−Schottky analysis will be called N_{MS} and the corresponding apparent built-in voltage is V_{MS}.

III. CHEMICAL CAPACITANCE

In the case of a Schottky contact between a doped semiconductor and a metal, the voltage modulates the width of the space charge region at the contact and the capacitance behaves like the capacitance of a flat plate capacitor with the width of the space charge region determining the value of the capacitance. In intrinsic or lowly doped materials, the capacitance is no longer dominated by the charge of the doping atoms, but instead it is dominated by the charge carriers injected from the contact. This capacitance is called chemical capacitance or diffusion capacitance and usually exceeds the space charge region capacitance at higher forward voltages.

Figure 2 shows a simulation of an intrinsic, 100 nm thick device with constant and small electron injection barrier at the cathode (barrier height φ_b = 100 meV) and a variable injection barrier at the anode, which allows us to see the transition from single carrier devices (low V_{bi}) to bipolar device (high V_{bi}). If the device has a sufficiently high built-in voltage V_{bi}, the chemical capacitance can drastically exceed the geometric capacitance. This behavior is different from single carrier devices where the injection of one carrier is suppressed by a high contact barrier.[38] Thus, the capacitance can no longer be understood easily in terms of plate capacitors. Instead, the capacitance depends on the increase of charge with voltage due to the injection of electrons and holes from their respective contacts. The exponential increase in electron concentration

dx.doi.org/10.1021/jp300397f | J. Phys. Chem. C XXXX, XXX, XXX−XXX

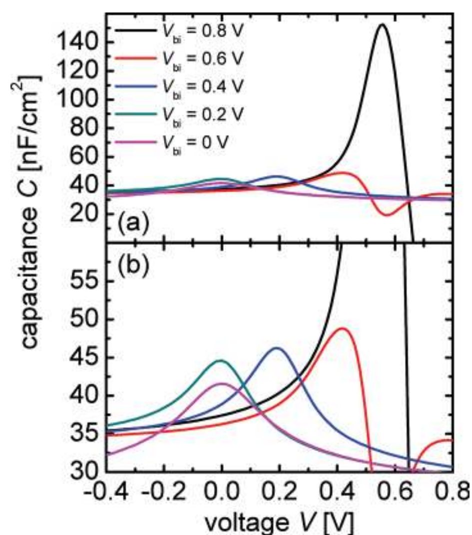

Figure 2. Simulated capacitance voltage spectra for a 100 nm thick cell where the cathode contact barrier has been fixed to 100 meV and the anode contact barrier for holes is varied from 100 to 900 meV. At 100 meV the cell is a bipolar diode with a high V_{bi} = 0.8 V, while toward higher hole barriers the hole injection becomes more difficult and the device becomes a single carrier device with lower V_{bi}. Only in the case of low injection barriers for electrons at the cathode and holes at the anode, the capacitance at forward bias exceeds the geometrical capacitance drastically. In the case of single carrier devices, the excess capacitance relative to the geometric capacitance is small as discussed in ref 38. Panels (a) and (b) show the same data but different capacitance ranges.

close to the cathode and hole concentration close to the anode leads to an exponential increase of the capacitance.[16]

The chemical capacitance in organic solar cells is similar in its voltage dependence to the space charge region capacitance and can therefore lead to misinterpretations of capacitance−voltage measurements. In the following we want to investigate under which circumstances the capacitance of the space charge region can be discriminated from the chemical capacitance and, thus, under which circumstances a safe determination of the doping density and the built-in voltage is possible.

IV. MODEL USED FOR THE SIMULATIONS

To investigate the sensitivity of the Mott−Schottky analysis, we perform steady state and frequency domain simulations with a drift-diffusion solver called SCAPS,[31−34] which has been developed by the group of M. Burgelman at the University of Gent. The software solves the continuity equations for electrons and holes as well as the Poisson equation that connects the charge with the electrical potential as discussed in more detail in the Supporting Information. After convergence of the steady state solution at a certain bias, a small signal analysis is performed that yields the complex admittance from which the capacitance is calculated.

In the following we will briefly discuss the boundary conditions used in the simulation. There are boundary conditions for the electrical potential and for the concentrations of electrons and holes. At zero volt applied bias, the difference between the electrical potential φ at the back and the front is the built-in voltage, that is, $V_{bi} = (\varphi(x = d) - \varphi(x = 0))/q$. In a typical band diagram, the electrical potential is not explicitly given, but the conduction and valence band edge follow the electrical potential as long as there is no abrupt offset at the interface to another material. Thus, $E_C = -\varphi$ + const. Since we only consider the active layer in Figure 1, the built-in voltage can be written as the difference between the conduction band edge E_C at the hole contact and at the electron contact at 0 V applied bias, that is, V_{bi} $(V = 0) = (E_C(V = 0, x = 0) - E_C(V = 0, x = d))/q$ as is shown in Figure 1. At an applied bias, the electrostatic potential difference is reduced correspondingly, that is, $V_{bi} - V = (\varphi(x = d) - \varphi(x = 0))/q$.

The concentration of the electrons and holes at a Schottky contact depend on the effective density of states N_C and N_V and on the value of the Schottky barrier height φ_b relative to the thermal energy kT. The equilibrium concentration of electrons at the back contact is

$$n_0(x = d) = N_C \exp\left(-\frac{\varphi_b(x = d)}{kT}\right) \tag{4}$$

and the equilibrium concentration of holes at the front contact is

$$p_0(x = 0) = N_V \exp\left(-\frac{\varphi_b(x = 0)}{kT}\right) \tag{5}$$

The equilibrium concentrations of the minority carriers are given everywhere by

$$n_0(x) = \frac{n_i^2}{p_0(x)} \tag{6}$$

where the intrinsic carrier concentration

$$n_i^2 = N_C N_V \exp\left(-\frac{E_g}{kT}\right) \tag{7}$$

is a function of the effective densities of states and the band gap E_g. The currents at the contact are a function of the excess carrier concentration and the so-called surface recombination velocities. There are four boundary conditions for the current densities J, namely,

$$J_n(0) = qS_{nf}(n(0) - n_0(0)) \tag{8a}$$

$$J_p(0) = qS_{pf}(p(0) - p_0(0)) \tag{8b}$$

$$J_n(d) = qS_{nb}(n(d) - n_0(d)) \tag{8c}$$

$$J_p(d) = qS_{pb}(p(d) - p_0(d)) \tag{8d}$$

where $S_{nf,b}$ is the surface recombination velocity for electrons at the front or back respectively, while $S_{pf,b}$ is the analogous quantity for the holes. While the surface recombination velocities for majority carriers (electrons at the back contact = cathode and holes at the front contact = anode) have to be high to ensure that current can flow at all, the surface recombination velocities for minorities (S_{nf} and S_{pb}) can be either high (nonselective contacts) or low (selective contacts).

In the case of flatband contacts, the equations for the current densities stay exactly the same, but the equilibrium concentrations now depend on the doping density and not on a Schottky barrier height. For flatband contacts, the space charge ρ at the contact is zero; thus, according to Poisson's equation the electrical potential is flat as seen in Figure 1a at the front contact. The concentration of electrons and holes at the flatband contact follows from the requirement of charge neutrality, $\rho = q(p - n - N_A) = 0$. Thus, if the p-type doping

density $N_A \gg n_i$, the equilibrium concentration of holes at the anode of a flatband contact is just $p_0 = N_A$, while n_0 follows again from eq 6.

V. SIMULATIONS

Usually, the CV scan leads to a straight line in reverse bias that has to be extrapolated to forward bias to obtain the built-in voltage. At forward bias, there are deviations from the straight line because the total capacitance is now influenced by the chemical capacitance[39] of the injected charge carriers and it is not anymore determined by the space charge region capacitance alone.

In organic solar cells with typical thicknesses of 100 nm, the space charge region capacitance at low forward or reverse bias saturates quickly at the minimum value given by the width of the active layer itself. It is therefore usually necessary to evaluate the CV scan at low forward biases, where the total capacitance is affected by contributions from the space charge region as well as from the chemical capacitance of the free carriers and where the depletion approximation is not necessarily appropriate. Whether or not the space charge region capacitance due to the doping of the organic film is dominant depends mainly on the thickness of the sample. Figure 3a shows an example of a simulation of a 100 nm thick semiconductor with parameters as given in Table 1 at a forward bias $V = 0.4$ V. The voltage is chosen such that it is close to the inclination point in the Mott−Schottky plot of the simulated cells, where one could fit a straight line to the data and determine the apparent doping density using eq 3. The electron and hole concentrations for the case of a completely intrinsic semiconductor and a semiconductor with an acceptor concentration $N_A = 5 \times 10^{15}$ cm^{-3} are compared. It is obvious that the doping density is not yet sufficient to substantially change the carrier concentrations between the two cases. Increasing the doping level by 1 order of magnitude leads to the situation shown in Figure 3b, where now in a large part of the device the electron concentration is orders of magnitude smaller than the hole concentration. If we determine the apparent doping density from the Mott−Schottky analysis of the three situations in Figure 3a,b, we obtain the doping profiles as shown in Figure 3c. For a doping density $N_A = 5 \times 10^{16}$ cm^{-3}, it is possible to determine the doping density relatively well ($N_{MS} \approx N_A$), while for $N_A = 5 \times 10^{15}$ cm^{-3} the apparent doping density is slightly above $N_{MS} = 1 \times 10^{16}$ cm^{-3}, which is identical to the situation without any doping. This means that for the chosen parameters, Mott−Schottky analysis is not sensitive to doping densities below $N_A \approx 1 \times 10^{16}$ cm^{-3}. Note that the conclusion of Figure 3 is nearly independent of the selectivity of the contact or the built-in voltage (i.e., the concentration of majorities at the contact). In the Supporting Information the graphs are shown for smaller concentrations of majorities and for selective and nonselective contacts.

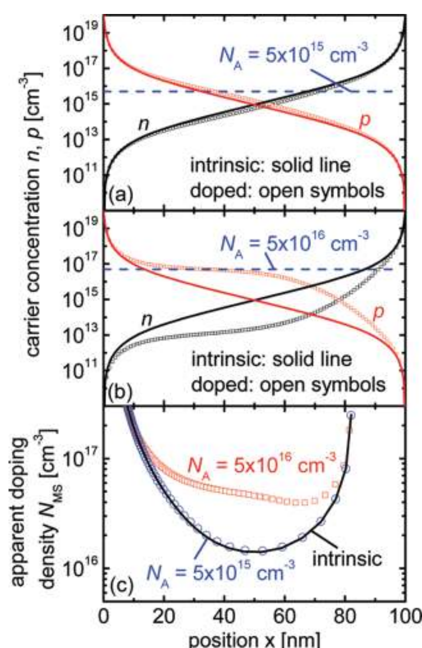

Figure 3. Carrier distribution in a solar cell with two Schottky contacts (like Figure 1b) comparing the cases of (a) $N_A = 5 \times 10^{15}$ cm^{-3} and (b) $N_A = 5 \times 10^{16}$ cm^{-3} with the intrinsic situation. Only in the latter case, the electron and hole concentration are substantially altered as compared to the intrinsic case. (c) Apparent doping densities as determined from Mott−Schottky analysis. Only in the case $N_A = 5 \times 10^{16}$ cm^{-3}, the doping density is correctly obtained from CV, while $N_A = 5 \times 10^{15}$ cm^{-3} is less than the apparent doping density of an intrinsic layer and thus not detectable.

Table 1. Parameters Used for the Simulations if Not Stated Otherwise[a]

	Default set
$\mu_n = \mu_p$ [cm^2/(V s)]	2×10^{-4}
$N_C = N_V$ [cm^{-3}]	10^{20}
E_g [eV]	1.0
k [cm^3 s^{-1}]	5×10^{-12}
$S_{nf} = S_{pb}$ [cm/s]	10^5
φ_b [meV]	0
ε_r	3.8

[a]The parameters are as indicated in the column labeled default set if not stated otherwise. All parameters are the same for electrons and holes except for the properties of the contacts and the doping density. The back contact is always a Schottky contact, and the front contact is a Schottky or a Flatband contact, depending on the simulation. The doping is always a shallow acceptor doping and the frequency used in the simulation is 1 kHz.

If we change the thickness of the device in our simulation to 1 μm, which is considerably thicker than most polymer:fullerene cells, we obtain the carrier concentrations as depicted in Figure 4a, and the apparent doping profiles as in Figure 4b. For the chosen parameters and $N_A = 5 \times 10^{15}$ cm^{-3}, the width of the space charge region is around 150 nm, which fits nicely into the 1 μm thick cell and is clearly visible at around $x = 850$ nm $= d - 150$ nm. For $x < 850$ nm, the concentration of holes for the doped device is the same as the doping density. For $x > 850$ nm, the hole concentration is decreased and the depletion approximation is valid at least close to the edge of the space charge region but not close to the contact, where the electron concentration is much larger than the doping density. Nevertheless, for the 1 μm thick cell, already the low doping leads to a drastic difference between the carrier concentration in the doped and undoped cases, and the doping density is accurately determined even though the depletion approximation is only valid close to the edge of the space charge region. The apparent doping density of the intrinsic film is now $N_{MS} \approx 1 \times 10^{14}$ cm^{-3}.

Our studies indicate that for every thickness, there is a range of doping levels that does not change the carrier distribution

dx.doi.org/10.1021/jp300397f | J. Phys. Chem. C XXXX, XXX, XXX−XXX

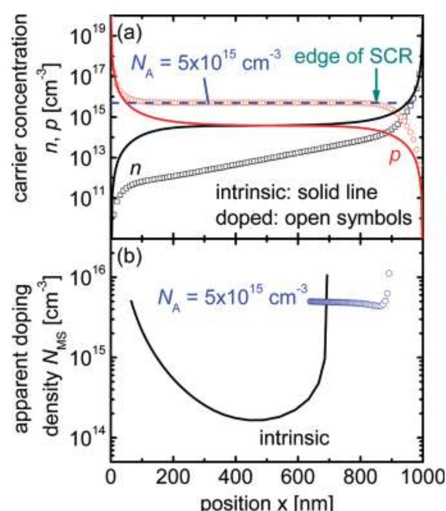

Figure 4. In the case of a 1 μm thick cell, a doping density $N_A = 5 \times 10^{15}$ cm^{-3} already affects the carrier concentration substantially (a) and the apparent doping density from Mott–Schottky analysis (b) correctly distinguishes between the doped and intrinsic cases.

substantially and is not detectable in Mott–Schottky analysis. In order for the doping level to be detectable, it must be higher than the apparent doping level that one would obtain from an intrinsic solar cell. Figure 5 presents this apparent doping

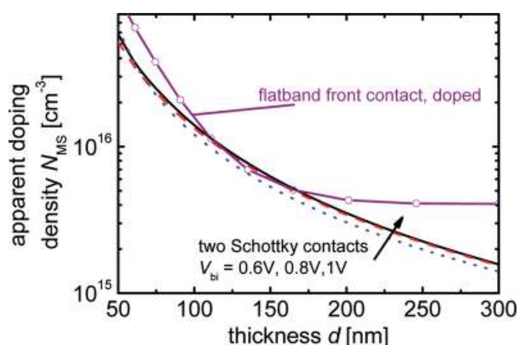

Figure 5. Apparent doping density as a function of active layer thickness for different scenarios. The lines without symbols correspond to a situation as shown in Figure.1b, with built-in voltages V_{bi} of 0.6 V(dotted line), 0.8 V (dashed line), and 1 V (solid line) and without any doping. The lines with symbols correspond to a situation as in Figure 1a with doping ($N_A = 5 \times 10^{15}$ cm^{-3}). The case with doping saturates at the correct doping density at high thicknesses, showing the general applicability of the method at higher thicknesses (and doping densities).

density as obtained from Mott–Schottky analysis of intrinsic devices with different thicknesses and built-in voltages (lines). It is obvious that the built-in voltage has only a minor effect on the apparent doping density and thus on the level of doping that the layer has to exceed to be detectable by Mott–Schottky analysis. In addition, Figure 6 shows one simulation for a situation as depicted in Figure 1a, where the front contact is a flatband contact, meaning that the distance between Fermi-level and valence band edge at the front contact is solely determined by the doping density and not by the properties of the front contact. In this situation, we obtain the line with open circles for a lowly doped sample with flatband front contact, where the apparent doping density saturates at its real doping level $N_A = 5 \times 10^{15}$ cm^{-3} for high thicknesses.

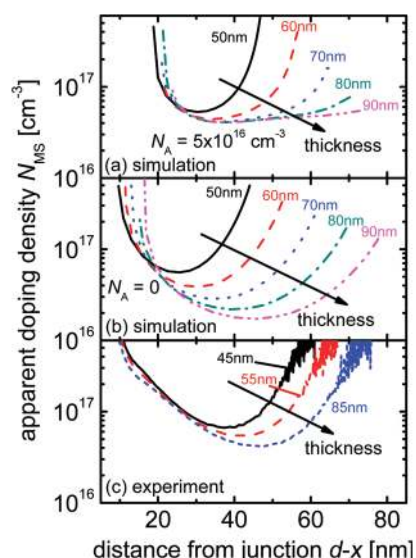

Figure 6. Comparison of simulations assuming the general band diagrams as given in Figure 1 with experimental data (c) on a set of P3HT/PCBM solar cells with thicknesses of 45 nm (solid line), 55 nm (dashed line), and 85 nm (short dashed line). The scheme in Figure 1a corresponds to simulation in Figure 6a and Figure 1b corresponds to 6b. The experimental data (c) as well as the simulations of the intrinsic cell in (b) show no plateau in the doping profile and a clear trend with thickness, which implies that the experimental results are not a good measure of doping in this case. Both experiment and simulation are done at a frequency of 1 kHz.

Note that the values for the apparent doping density in Figure 5 are taken from the minimum of the doping profiles at the different thicknesses. This implies that fitting the Mott–Schottky plots with straight lines can easily lead to higher apparent doping densities if the straight line is not fitted to the inclination point, where the slope of C^{-2} vs V is greatest and the doping density is lowest.

VI. COMPARISON: SIMULATION – EXPERIMENT

In the following, we want to compare simulations of the capacitance of the two types of band diagrams depicted in Figure 1 with experimental results on a series of ITO/PEDOT:PSS/P3HT:PCBM/(Ca)/Al solar cells which were measured and evaluated in the same manner as the simulations to yield the apparent doping profiles as shown in Figure 6. Figure 6a shows the simulation for a device with flatband front contact and a doping density of $N_A = 5 \times 10^{16}$ cm^{-3} for thicknesses of 50–90 nm (in 10 nm steps). For low thicknesses, the doping density cannot be accurately determined but for 80 and 90 nm, the doping profile has a plateau, where the evaluation of the doping density is possible. In contrast, the intrinsic devices with Schottky junctions on both sides never show a plateau (Figure 6b). The lack of a plateau, therefore, seems to be a good indication that the apparent doping density is not reliable. The experimental data (Figure 6c) of several devices with nominal thicknesses of 45, 55 and 85 nm (as determined from profilometer measurements) show a behavior similar to the simulations of the intrinsic devices. The doping densities are slightly higher than in the simulation, but there is still a clear trend with thickness that one would not expect if the apparent doping density from the Mott–Schottky analysis corresponded to a real doping density. In addition, the apparent doping profiles are curved

just as the simulations of the intrinsic devices. Thus, we conclude that for these thin samples, the Mott–Schottky analysis does not reliably determine doping density. The samples could be undoped or doped at a level equal or lower than the values from the Mott–Schottky analysis.

For thicker samples, however, the determination of doping densities may become possible depending on the level of doping present in the device. Figure 7 shows two comparably thick P3HT/PCBM devices fabricated in different laboratories, from different polymer batches and with different electrodes. Details on the preparation of the samples are presented in the Experimental Details. Sample A ($d \approx 320$ nm) shows a similar behavior as the thinner cells in Figure 6, namely, a Mott–Schottky plot (Figure 7a) with an inclination point and a doping profile that looks comparable to the simulated doping profiles of undoped cells shown, for example, in Figures 3b, 4b, and 6b. The doping profile has a minimum value around $N_{MS} \approx 3 \times 10^{15}$ cm^{-3}, which roughly defines the upper limit for the doping density in this device. Thus, sample A is either intrinsic or has a doping density smaller than $N_{MS} \approx 3 \times 10^{15}$ cm^{-3}.

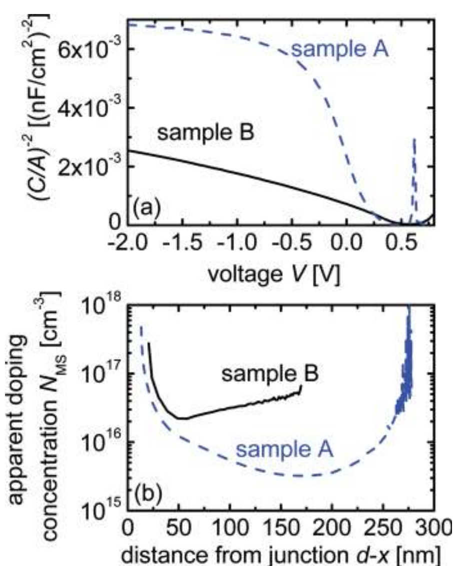

Figure 7. Experimental data derived from capacitance voltage measurements of two thick P3HT/PCBM cells at 1 kHz. Sample A ($d \approx 320$ nm) shows a Mott–Schottky plot (a) that does not show a clear straight region that is unaffected by the saturation of the capacitance at high and low voltages. Thus it does not give a reliable value of doping (b) but just an upper limit of $N_{MS} < 3 \times 10^{15}$ cm^{-3}. In contrast, sample B ($d \approx 250$ nm) shows a nearly straight Mott–Schottky plot (a) over a 2.5 V range, which translates in a comparably flat doping profile (b). The doping density is around $N_{MS} \approx 3 \times 10^{16}$ cm^{-3} for sample B.

Sample B ($d \approx 250$ nm), however, shows a different behavior in the Mott–Schottky plot in Figure 7a. The plot of C^{-2} is nearly a straight line from small forward voltages up to negative voltages as expected for doped samples. Consequently it is now possible to determine the doping density in sample B by applying eq 3 to the data in Figure 7a. The derived doping profile in Figure 7b suggests a doping density of around $N_{MS} \approx 3 \times 10^{16}$ cm^{-3}. The reason for the differences between samples A and B is unclear and of no relevance to the point we aim to make in this article. The comparison shows, however, how large the differences in doping in one material system can be and how a safe determination of doping looks in comparison to a sample, where the doping density is too low to be quantifiable by Mott–Schottky analysis, which can then only provide an upper limit.

Some measurements in the literature[17,40] show behavior similar to sample B insofar as a straight line over a larger range of voltages including reverse bias is visible in Mott–Schottky plots. It is important to point out that in all cases where a straight line over a range of negative voltages is seen, the cell has a sufficiently high thickness to make reliable determinations of doping densities possible.

VII. THE DISADVANTAGES OF LOW BUILT-IN VOLTAGES

In order to work, solar cells need a built-in asymmetry. This asymmetry can be realized entirely by selective contacts due to, for example, abrupt band offsets at the contacts.[41,42] If the electron contact (cathode) is unable to extract holes and vice versa, the solar cell will work even without any built-in voltage, that is, change in electrostatic potential. The current is then solely driven by the gradients in carrier concentration, that is, by diffusion. While the solar cell will work without a built-in potential, it cannot work efficiently without it. This is due to the fact that at forward voltages higher than the built-in voltage, the net field in the device reverses, thereby impeding charge carrier extraction instead of helping it. Although diffusion alone can be sufficient to transport charge carriers to the contacts, diffusion against an electric field is generally inefficient if the electric field is too high and the carrier mobility is too low.[42] This negative impact of the electric field in devices with low built-in voltages automatically leads to low fill factors and even S-shapes if the barrier for extraction becomes too large.

Figure 8 illustrates these effects for one example of a 150 nm thick cell with a flatband front contact and a back contact with a Schottky-junction (as depicted in Figure 1a in the paper). Note that the contacts are perfectly selective; that is, holes cannot leave the device at the cathode and electrons cannot leave at the anode. The optical generation rate is constant and given by $G = 4 \times 10^{21}$ cm^{-3} s^{-1}. All the other parameters are as given in Table 1 in the paper. Since recombination is only determined by recombination at the internal donor–acceptor interface and not at the contacts, the open-circuit voltage does not depend on the built-in voltage. However, the fill factor FF drops drastically once the built-in voltage drops below the open-circuit voltage.

In the case of nonselective contacts, the FF will stay roughly constant and the open circuit voltage will decrease, because in this case the open circuit voltage will be deteriorated by recombination at the contacts (electrons recombine at the anode and holes recombine at the cathode). While it is unclear, whether the contacts in typical organic solar cells should be rather considered selective or nonselective, a built-in voltage that is smaller than the open-circuit voltage will have an effect on either FF or V_{oc} or both, which means that solar cells with a high FF will most likely have a V_{bi} that is larger than V_{oc}. The fact that electrodes can have an effect on V_{oc} if they are not optimized is supported by investigations of different electrode materials[43] as well as of studies on the effect of interface layers[44−47] between the blend and the metal back contact which often have a positive effect on the open circuit voltage. Thus, it is reasonable to investigate the possible errors when determining the built-in voltage from the Mott–Schottky analysis.

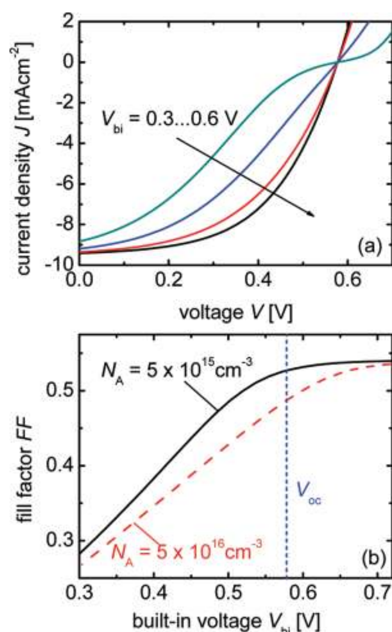

Figure 8. (a) Current/voltage curves as a function of built-in voltage V_{bi} simulated for a 150 nm thick active layer with a flatband front contact and a Schottky contact at the back. The built-in voltage is changed by changing the Schottky barrier at the back contact. The parameters for the simulation are as given in Table 1 and the doping density is $N_A = 5 \times 10^{15}$ cm^{-3}. (b) FF as a function of built-in voltage for two different doping densities (all other parameters as for (a)). A reduction of V_{bi} below the open circuit voltage immediately leads to a loss in FF caused by carrier diffusion against the electric field.

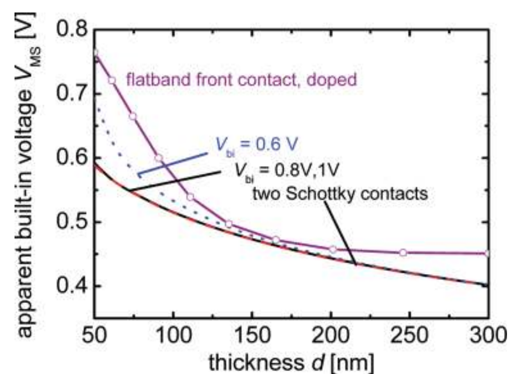

Figure 9. Apparent built-in voltage V_{MS} as a function of active layer thickness for the devices with different boundary conditions, which are identical to the ones used in Figure 5. In all cases, the apparent built-in voltage from the Mott–Schottky analysis does not correctly reproduce the actual built-in voltage since the depletion approximation is not valid for lowly doped devices.

VIII. THE BUILT-IN VOLTAGE AND THE DEPLETION APPROXIMATION

The built in voltage as determined from Mott–Schottky analysis is known to give rather low values in the 400 mV range for P3HT/PCBM that seem to be in contrast to the typical open circuit voltages of 600 mV or slightly below. In addition, a recent study[48] found that the experimental value for the built-in voltage is thickness dependent, which will be explained in the following as a measurement artifact using similar arguments as before for the thickness dependence of the doping density.

If we fit a straight line to the inclination point of the C^{-2} vs V relation according to

$$C^{-2} = \frac{2(V_{bi} - V)}{q\varepsilon A^2 N_A} \quad (9)$$

we obtain the built-in voltage from the intersect with the voltage axis. The measurements presented in Figure 6c lead to built-in voltages in a narrow range around V_{bi} = 300 mV, which is much lower than the corresponding one sun open circuit voltages ($V_{oc} \approx$ 600 mV). We have already shown that the Mott–Schottky analysis is not appropriate for the determination of the doping density in lowly doped thin films. Thus, it is not surprising that the built-in voltage is not accurate as well. Figure 9 gives examples on which parameters the apparent built-in voltage from the Mott–Schottky analysis depends and shows how insensitive the apparent built-in voltage in thin films is on the actual built-in voltage. Note that the latter is an input parameter in the simulation and defined as $qV_{bi} = E_g - \varphi_b$(cathode) $- \varphi_b$(anode). The data in Figure 9 correspond directly to the doping density data shown in Figure 5. The lines without symbols are a simulation of a set of three intrinsic cells with a Schottky junction on both sides, no traps, and a built-in voltage of 0.6 V, 0.8 V, and 1 V. The cases of V_{bi} = 0.8 and 1 V are essentially identical, while the case of V_{bi} = 0.6 V has a slightly increased apparent built in voltage V_{MS} at lower thicknesses. The trend in V_{bi} is therefore not at all reproduced and the variations due to thickness differences are much larger than the differences between the simulations at different V_{bi} and one thickness. The simulation with a flatband front contact shows a similar trend with lower V_{bi} at higher thicknesses. Interestingly, even the combination of thick layer (300 nm), sufficiently high doping density ($N_A = 5 \times 10^{15}$ cm^{-3}), and flatband front contact does not lead to a correct determination of the real V_{bi}. The reason for this is that the determination of V_{bi} is even more sensitive to the validity of the depletion approximation than the determination of the doping density. The depletion approximation assumes that the charge is entirely due to the doping and there are no free carriers in the space charge region. Close to the metal back contact however, electrons are injected and lead to a higher charge density close to the metal contact, as can be seen, for example, in Figures 3a,b or 4a. The real built-in voltage depends on the charge close to the contact, but the apparent built-in voltage is not affected by it, because it is calculated from a theory which neglects this extra charge. Thus, the actual built-in voltage in both situations shown in Figure 1 can be much higher than the apparent built-in voltage determined from the Mott–Schottky analysis.

In all cases, V_{MS} decreases as a function of thickness as seen in experiments as well.[48] This trend is directly connected to the doping density trend discussed in the first part of the paper. At low thicknesses, the influence of the electrode capacitance becomes larger and the C^{-2} bends over already around short circuit or at small negative bias (cf. sample A in Figure 7a). The slope of the $C^{-2}(V)$ curve is then not only determined by the doping density but also by the thickness, which controls the saturation level at negative voltages. The change in slope leads directly to a change in doping density according to eq 3. The change in slope also leads to a change in the intersection with the voltage-axis. A reduction in slope (= higher apparent doping density) by the saturation regime shifts the voltage-axis intersect to higher voltages and leads to a higher V_{MS}.

Figure 10 shows a comparison of the apparent built-in voltage V_{MS} as determined from the Mott–Schottky analysis and the real built-in voltage V_{bi}, which enters the simulation as a parameter. In the case of the simulation with a flatband front contact, the Schottky barrier at the back contact is varied, while the valence band edge to hole Fermi-level distance at the front contact is fixed due to a doping density of $N_A = 5 \times 10^{15}$ cm^{-3}. The maximum built-in voltage is then $V_{bi} = 0.74$ V for the parameters as given in Table 1 and a thickness of 1 μm to avoid any problems due to thin layers as discussed above. Increasing the Schottky barrier at the back contact (i.e., lowering V_{bi}) first does not have any effect on V_{MS} which is fixed at just below 0.5 V. Only at sufficiently high Schottky barriers is the concentration of electrons at the back contact lower than $N_A = 5 \times 10^{15}$ cm^{-3} and the depletion approximation is finally valid. Only under these conditions the apparent and actual V_{bi} converge.

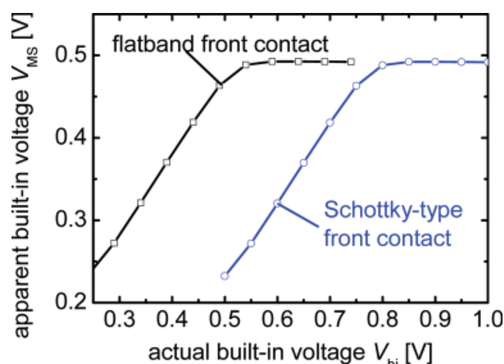

Figure 10. Comparison of the actual built-in voltage used in the simulation and the apparent built-in voltage V_{MS} determined from the Mott–Schottky analysis of the simulated capacitance voltage curve at 1 kHz. In case of a flatband front contact, the correct built-in voltage is reproduced in cases where the charge of the doping atoms dominates the total charge in the space charge region at the (Schottky type) back contact. In case of a Schottky contact on both sides, the Mott–Schottky analysis is insensitive to the band bending at the front contact which is entirely due to injection of holes from the contact and independent of the charge of the doping molecules.

In the case of two Schottky junctions, band bending at the front contact is entirely due to holes injected from the front contact and has nothing to do with the doping density. The Mott–Schottky analysis is almost completely insensitive to this second space charge region, and the resulting apparent V_{bi} curve is shifted with respect to the case of no band bending by a constant amount, which represents the band bending (260 mV in this case) at the front contact.

IX. CONCLUSIONS

The simulations presented in this article show that Mott–Schottky analysis relies on the depletion approximation, which is not a safe assumption in layers that are either too thin or too lowly doped to neglect the free carriers injected from the electrodes. To quantify the range of doping densities and thicknesses where the Mott–Schottky analysis is safe to use, we calculate the apparent doping density of intrinsic films as a function of thickness for various boundary conditions. In all cases, we obtain similar values of the apparent doping density as a function of thickness, which indicate that apparent doping densities $N_{MS} > 10^{16}$ cm^{-3} from the Mott–Schottky analysis are consistent with totally intrinsic active layers if the thickness of the layer is below 100 nm. Experimental data show a similar trend with thickness as the simulations, albeit on a slightly higher level. From comparison with simulations, we conclude that the correct determination of the doping density is not possible from these thin devices. However, for thicker and/or more heavily doped devices, the determination of the doping density from the Mott–Schottky analysis becomes more reliable. The determination of the built-in voltage is particularly sensitive to violations of the depletion approximation, which implies that even for slightly thicker, doped samples, the determination of the built-in voltage from Mott–Schottky plots is difficult to accurately ascertain.

■ EXPERIMENTAL DETAILS

Sample A and the samples with thicknesses under 100 nm were prepared as follows. P3HT was purchased from Merck and PCBM from Nano-C. Patterned ITO was cleaned in detergent, acetone, and isopropanol. The PEDOT:PSS(Al4083) layer was spin coated onto the ITO substrates with a thickness of ~35 nm and annealed at 150 °C for 20 min. Subsequently, the P3HT:PCBM layer solution (Sample A dissolved in chlorobenzene (CB) at 1:1 wt %, 50 mg/mL); samples with thicknesses under 100 nm (dissolved in chlorobenzene (CB) at 1:1 wt %, 30 mg/mL)) was spin-coated on top. Aluminum was evaporated at 5.0–5.5 × 10^{-6} mbar as cathode. At last all samples were postannealed for 20 min at 150 °C in a nitrogen-filled glovebox.

Sample B was prepared as follows. The PEDOT:PSS layer (CLEVIOS P VP Al 4083) was spin coated to a thickness of ~30 nm and annealed at 140 °C for 15 min. The active layer in was fabricated using a 1:1 wt. ratio of P3HT to PCBM in a 20 mg/mL (each component) dichlorobenzene solution. The P3HT used was Plexcore OS 2100 purchased from Aldrich (CAS RN 104934-50-1), and the PCBM was purchased from Nano-C (Batch BJ101112). This solution was spin coated under the necessary conditions to achieve a ~250 nm active-layer thickness. Upon completion of spin coating, the (still wet) active layer film was placed under a 3" diameter Petri dish to slowly dry ($t_{dry} \approx 20$ min). After drying, the sample was annealed for 10 min at 110 °C and loaded into a thermal evaporator. A Ca/Al top electrode was evaporated onto the device at 2.1–2.5 × 10^{-6} mbar by first allowing ~15 nm of Ca to deposit onto the shutter before exposing the devices, and then opening to deposit 20 nm of Ca at a rate of 0.5 Å/s. Immediately following the Ca evaporation, 100 nm Al was deposited at a rate of 1.0 Å/s to yield the final Ca (20 nm)/Al (100 nm) top electrode. For verification purposes, the devices (A = 4.5 mm^2) were tested under simulated AM 1.5G illumination and had values of the order short circuit current density J_{sc} = 8.7 mA/cm^2, open circuit voltage V_{oc} = 0.57 V, fill factor FF = 60%, and power conversion efficiency η = 3.0%.

■ ASSOCIATED CONTENT

Ⓢ Supporting Information

More information about the drift-diffusion model used as well as simulations on the effect of the injection barriers at cathode and anode on the carrier distribution and simulations on the effect of a grading in the density of doping atoms and the dielectric constant on the determination of doping densities. In addition, we show simulations on the thickness dependence of the apparent built-in voltage. This material is available free of charge via the Internet at http://pubs.acs.org.

AUTHOR INFORMATION

Corresponding Author

*E-mail: t.kirchartz@imperial.ac.uk.

Notes

The authors declare no competing financial interest.

ACKNOWLEDGMENTS

The authors would like to thank Juan Bisquert (Castelló), Jennifer Heath (Linfield), Marc Burgelman, and Koen Decock (Gent) for valuable discussions and advice. T.K. acknowledges support by an Imperial College Junior Research Fellowship. W.G. acknowledges support from P. R. China's State Scholarship Fund. S.A.H. and Y.Y. would like to thank the NSF IGERT: Materials Creation Training Program (MCTP) - DGE-0654431, the California NanoSystems Institute, and the Office of Naval Research (N00014-04-1-0434, Program Manager: Dr. P. Armistead) for financial support of this research.

REFERENCES

(1) Brabec, C. J.; Heeney, M.; McCulloch, I.; Nelson, J. *Chem. Soc. Rev.* **2011**, *40*, 1185−1199.
(2) Brabec, C. J.; Gowrisanker, S.; Halls, J. J. M.; Laird, D.; Jia, S. J.; Williams, S. P. *Adv. Mater.* **2010**, *22*, 3839−3856.
(3) Clarke, T. M.; Durrant, J. R. *Chem. Rev.* **2010**, *110*, 6736−6767.
(4) Blom, P. W. M.; Mihailetchi, V. D.; Koster, L. J. A.; Markov, D. E. *Adv. Mater.* **2007**, *19*, 1551−1566.
(5) Deibel, C.; Strobel, T.; Dyakonov, V. *Adv. Mater.* **2010**, *22*, 4097−4111.
(6) Deibel, C.; Dyakonov, V. *Rep. Prog. Phys.* **2010**, *73*, 096401.
(7) Glatthaar, M.; Riede, M.; Keegan, N.; Sylvester-Hvid, K.; Zimmermann, B.; Niggemann, M.; Hinsch, A.; Gombert, A. *Sol. Energy Mater Sol. Cells* **2007**, *91*, 390−393.
(8) Fabregat-Santiago, F.; Garcia-Belmonte, G.; Mora-Sero, I.; Bisquert, J. *Phys. Chem. Chem. Phys.* **2011**, *13*, 9083−9118.
(9) Bisquert, J.; Garcia-Belmonte, G. *J. Phys. Chem. Lett.* **2011**, *2*, 1950−1964.
(10) Heath, J.; Zabierowski, P. In *Advanced Characterization Techniques for Thin Film Solar Cells*; Abou-Ras, D., Kirchartz, T., Rau, U., Eds.; Wiley-VCH: Weinheim, 2011; pp 81−105.
(11) Heath, J. T.; Cohen, J. D.; Shafarman, W. N. *J. Appl. Phys.* **2004**, *95*, 1000−1010.
(12) Abdou, M. S. A.; Orfino, F. P.; Son, Y.; Holdcroft, S. *J. Am. Chem. Soc.* **1997**, *119*, 4518−4524.
(13) Boix, P. P.; Garcia-Belmonte, G.; Munecas, U.; Neophytou, M.; Waldauf, C.; Pacios, R. *Appl. Phys. Lett.* **2009**, *95*, 233302.
(14) Bisquert, J.; Garcia-Belmonte, G.; Munar, A.; Sessolo, M.; Soriano, A.; Bolink, H. J. *Chem. Phys. Lett.* **2008**, *465*, 57−62.
(15) Boix, P. P.; Ajuria, J.; Etxebarria, I.; Pacios, R.; Garcia-Belmonte, G.; Bisquert, J. *J. Phys. Chem. Lett.* **2011**, *2*, 407−411.
(16) Garcia-Belmonte, G.; Boix, P. P.; Bisquert, J.; Sessolo, M.; Bolink, H. J. *Sol. Energy Mater. Sol. Cells* **2010**, *94*, 366−375.
(17) Garcia-Belmonte, G.; Munar, A.; Barea, E. M.; Bisquert, J.; Ugarte, I.; Pacios, R. *Org. Electron.* **2008**, *9*, 847−851.
(18) Glatthaar, M.; Mingirulli, N.; Zimmermann, B.; Ziegler, T.; Kern, R.; Niggemann, M.; Hinsch, A.; Gombert, A. *Phys. Status Solidi A* **2005**, *202*, R125−R127.
(19) Deibel, C.; Wagenpfahl, A.; Dyakonov, V. *Phys. Status Solidi R* **2008**, *2*, 175−177.
(20) Limpinsel, M.; Wagenpfahl, A.; Mingebach, M.; Deibel, C.; Dyakonov, V. *Phys. Rev. B* **2010**, *81*, 085203.
(21) Kirchartz, T.; Pieters, B. E.; Kirkpatrick, J.; Rau, U.; Nelson, J. *Phys. Rev. B* **2011**, *83*, 115209.
(22) Wagenpfahl, A.; Rauh, D.; Binder, M.; Deibel, C.; Dyakonov, V. *Phys. Rev. B* **2010**, *82*, 115306.
(23) Koster, L. J. A.; Smits, E. C. P.; Mihailetchi, V. D.; Blom, P. W. M. *Phys. Rev. B* **2005**, *72*, 085205.
(24) Kirchartz, T.; Pieters, B. E.; Taretto, K.; Rau, U. *Phys. Rev. B* **2009**, *80*, 035334.
(25) Blakesley, J. C.; Greenham, N. C. *J. Appl. Phys.* **2009**, *106*, 034507.
(26) MacKenzie, R. C. I.; Kirchartz, T.; Dibb, G. F. A.; Nelson, J. *J. Phys. Chem. C* **2011**, *115*, 9806−9813.
(27) Mihailetchi, V. D.; Koster, L. J. A.; Hummelen, J. C.; Blom, P. W. M. *Phys. Rev. Lett.* **2004**, *93*, 216601.
(28) Schafer, S.; Petersen, A.; Wagner, T. A.; Kniprath, R.; Lingenfelser, D.; Zen, A.; Kirchartz, T.; Zimmermann, B.; Wurfel, U.; Feng, X. J. *Phys. Rev. B* **2011**, *83*, 165311.
(29) Blakesley, J. C.; Neher, D. *Phys Rev B* **2011**, *84*, 075210.
(30) Xu, Z.; Chen, L. M.; Chen, M. H.; Li, G.; Yang, Y. *Appl. Phys. Lett.* **2009**, *95*, 013301.
(31) Burgelman, M.; Nollet, P.; Degrave, S. *Thin Solid Films* **2000**, *361*, 527−532.
(32) Burgelman, M.; Verschraegen, J.; Degrave, S.; Nollet, P. *Prog. Photovoltaics* **2004**, *12*, 143−153.
(33) Pieters, B. E.; Decock, K.; Burgelman, M.; Stangl, R.; Kirchartz, T. In *Advanced Characterization Techniques for Thin Film Solar Cells*; Wiley-VCH Verlag GmbH & Co. KGaA: New York, 2011; pp 501−527.
(34) Decock, K.; Khelifi, S.; Buecheler, S.; Pianezzi, F.; Tiwari, A. N.; Burgelman, M. *J. Appl. Phys.* **2011**, *110*, 063722.
(35) Khelifi, S.; Decock, K.; Lauwaert, J.; Vrielinck, H.; Spoltore, D.; Piersimoni, F.; Manca, J.; Belghachi, A.; Burgelman, M. *J. Appl. Phys.* **2011**, *110*, 094509.
(36) Li, G.; Shrotriya, V.; Huang, J. S.; Yao, Y.; Moriarty, T.; Emery, K.; Yang, Y. *Nat. Mater.* **2005**, *4*, 864−868.
(37) Kim, Y.; Cook, S.; Tuladhar, S. M.; Choulis, S. A.; Nelson, J.; Durrant, J. R.; Bradley, D. D. C.; Giles, M.; McCulloch, I.; Ha, C. S. *Nat. Mater.* **2006**, *5*, 197−203.
(38) van Mensfoort, S. L. M.; Coehoorn, R. *Phys. Rev. Lett.* **2008**, *100*, 086802.
(39) Bisquert, J. *Phys. Chem. Chem. Phys.* **2003**, *5*, 5360−5364.
(40) Morfa, A. J.; Nardes, A. M.; Shaheen, S. E.; Kopidakis, N.; van de Lagemaat, J. *Adv. Funct. Mater.* **2011**, *21*, 2580−2586.
(41) Rau, U.; Kron, G.; Werner, J. H. *J. Phys. Chem. B* **2003**, *107*, 13547−13550.
(42) Kirchartz, T.; Rau, U. In *Advanced Characterization Techniques for Thin Film Solar Cells*; Abou-Ras, D., Kirchartz, T., Rau, U., Eds.; Wiley-VCH Verlag GmbH & Co. KGaA: New York, 2011; pp 1−32.
(43) Brabec, C. J.; Cravino, A.; Meissner, D.; Sariciftci, N. S.; Fromherz, T.; Rispens, M. T.; Sanchez, L.; Hummelen, J. C. *Adv. Funct. Mater.* **2001**, *11*, 374−380.
(44) Asadi, K.; de Bruyn, P.; Blom, P. W. M.; de Leeuw, D. M. *Appl. Phys. Lett.* **2011**, *98*, 183301.
(45) He, Z. C.; Zhong, C. M.; Huang, X.; Wong, W. Y.; Wu, H. B.; Chen, L. W.; Su, S. J.; Cao, Y. *Adv. Mater.* **2011**, *23*, 4636.
(46) Seo, J. H.; Gutacker, A.; Sun, Y. M.; Wu, H. B.; Huang, F.; Cao, Y.; Scherf, U.; Heeger, A. J.; Bazan, G. C. *J. Am. Chem. Soc.* **2011**, *133*, 8416−8419.
(47) Ahlswede, E.; Hanisch, J.; Powalla, M. *Appl. Phys. Lett.* **2007**, *90*, 163504.
(48) Mingebach, M.; Deibel, C.; Dyakonov, V. *Phys. Rev. B* **2011**, *84*, 153201.